Ultrasound in Med. & Biol., Vol. 48, No. 9, pp. 1720–1732, 2022

0301-5629/$ - see front matter

https://doi.org/10.1016/j.ultrasmedbio.2022.04.216

● *Original Contribution*

MATERIAL PROPERTIES, DISSOLUTION AND TIME EVOLUTION OF PEGYLATED LIPID-SHELLED MICROBUBBLES: EFFECTS OF THE POLYETHYLENE GLYCOL HYDROPHILIC CHAIN CONFIGURATIONS

ROOZBEH H. AZAMI,* MITRA ALIABOUZAR,* JENNA OSBORN,* KRISHNA N. KUMAR,* FLEMMING FORSBERG,† JOHN R. EISENBREY,† SANKU MALLIK,‡ and KAUSIK SARKAR*

* Department of Mechanical and Aerospace Engineering, The George Washington University, Washington, DC, USA; † Department of Radiology, Thomas Jefferson University, Philadelphia, Pennsylvania, USA; and ‡ Department of Pharmaceutical Sciences, North Dakota State University, Fargo, North Dakota, USA

(*Received* 6 *October* 2021; *revised* 21 *March* 2022; *in final form* 21 *April* 2022)

Abstract—Polyethylene glycol (PEG) is often added to the lipid coating of a contrast microbubble to prevent coalescence and improve circulation. At high surface density, PEG chains are known to undergo a transition from a mushroom configuration to an extended brush configuration. We investigated the effects of PEG chain configuration on attenuation and dissolution of microbubbles by varying the molar ratio of the PEGylated lipid in the shell with three (0%, 2% and 5%) in the mushroom configuration and two (10% and 20%) in the brush configuration. We measured attenuation through the bubble suspensions and used it to obtain the characteristic rheological properties of their shells according to two interfacial rheological models. The interfacial elasticity was found to be significantly lower in the brush regime (~0.6 N/m) than in the mushroom regime (~1.3 N/m), but similar in value within each regime. The dissolution behavior of microbubbles under acoustic excitation inside an air-saturated medium was studied by measuring the time-dependent attenuation. Total attenuation recorded a transient increase because of growth resulting from air influx and an eventual decrease caused by dissolution. Microbubble shell composition with varying PEG concentrations had significant effects on dissolution dynamics. (E-mail: sarkar@gwu.edu)

Key Words: **Phospholipid-shelled microbubbles, Polyethylene glycol configuration, Microbubble dissolution, Acoustic response, Rheological properties, Interfacial elasticity, Exponential elasticity model, Ultrasound, Time-dependent attenuation.**

INTRODUCTION

Microbubbles coated by a shell of surface-active substances such as lipids and proteins are well-known contrast agents for ultrasound imaging. Because of their compressive gas core, these microbubbles oscillate in response to an acoustic wave and generate fundamental as well as various harmonic responses (de Jong et al. 2002; Katiyar and Sarkar 2011; Azmin et al. 2012; Paul et al. 2014; Helfield 2019). They could also act as potential drug carriers with drugs loaded in the core or on the shell, which can be released at the desired region in a controlled way by using external acoustic excitation (Marik et al. 2007; Kooiman et al. 2014; Mulvana et al. 2017). Such applications warrant stable microbubbles with a long circulation lifetime inside the body. Polyethylene glycol (PEG) is commonly incorporated into the microbubble shells to improve circulation by protecting them against macromolecule absorption and coalescence by creating a steric barrier of hydrophilic chains of the grafted PEG (Chen and Borden 2010). In addition, PEG chains can allow the linkage of drugs to the shell (Mulvana et al. 2017). Here, we investigate the effects of PEG concentrations on the behaviors of microbubbles, specifically how they change the shell properties, which in turn affect bubble dissolution and their acoustic responses.

Polyethylene glycol is a long-chain molecule, which when absorbed at an interface can take two different configurations, brush and mushroom, depending on the PEG molecular weight and its surface concentration (de Gennes 1987). If the surface concentration is high enough so that the distance between chains (D) is smaller than the Flory radius of the grafted PEG chain (R_F), the

Address correspondence to: Kausik Sarkar, The George Washington University, 800 22nd Street NW, Suite 3000, Washington DC 20052, USA. E-mail: sarkar@gwu.edu

chains extend and form a brush configuration ($D < R_F$). For lower PEG concentrations, the distance between chains is higher than the Flory radius; therefore, PEG chains form a mushroom-like configuration ($D > R_F$) (de Gennes 1987; Kenworthy et al. 1995). These alterations in PEG chain configuration and the shell chemistry, as we will discuss, have profound effects on the encapsulation properties, in turn determining the microbubbles' behavior under acoustic excitation.

The stability of microbubbles in a multigas medium is dependent on the shell properties. Permeability of the encapsulation to the gas core and the dissolved gas in the surrounding liquid can change the life span of microbubbles from seconds to hours (Sarkar et al. 2009; Kwan and Borden 2010). On the other hand, shell properties also critically determine the acoustic response of a microbubble. Therefore, an optimized balance between the acoustic response and the stability of microbubbles is highly desirable for maximizing their performance and clinical usability. This requires a proper understanding of the relation between shell chemistry and its stability and mechanical properties.

Shell composition can alter its material properties and, in turn, the acoustic response and stability of microbubbles (de Jong et al. 2002; van der Meer et al. 2007; Sboros 2008). Several models have been proposed to model the response of a microbubble to an acoustic pressure wave. Considering that the protective coatings of surface-active molecules are only a few molecules thick, our group has proposed an interfacial rheological model to account for its effects (Chatterjee and Sarkar 2003), which subsequently became a standard approach. Over the years, we and others have developed several different interfacial rheological models in terms of interfacial material properties such as interfacial elasticity, interfacial viscosity and surface tension and applied them to experimental observations to estimate the properties of the microbubble coating (Chatterjee and Sarkar 2003; Marmottant et al. 2005; Sarkar et al. 2005; Paul et al. 2010, 2013; Doinikov and Bouakaz 2011; Kumar and Sarkar 2016). In addition, direct measurement methods, such as the Langmuir trough (Lozano and Longo 2009), atomic force microscopy (AFM) (Sboros et al. 2006) and photoacoustic technique (Lum et al. 2016), have been used.

The stiffness of the lipid encapsulation of microbubbles has been reported to follow different trends with increasing PEG concentration in the shell in previous studies. , Dicker et al. (2013b) reported that the elasticity of the shell decreases when the 1, 2-distearoyl-*sn*-glycero-3-phosphoethanolamine−poly(ethylene glycol) (DSPE-PEG, molecular weight: 2000 to 5000) concentration in distearoylphosphatidylcholine (DSPC) microbubble shell changes from 1% to 7.5% molar ratio. However, Segers et al. (2018) reported insignificant changes in shell elasticity for dipalmitoylphosphatidylcholine (DPPC)−shelled microbubbles with 5%, 7.5% and 10% dipalmitoylphosphoethanolamine-polyethylene glycol-5000 (DPPE-PEG5000). Abou-Saleh et al. (2014) used AFM to measure the stiffness of microbubbles with DPPC shell mixed with DSPE-B-PEG2000 in molar fractions ranging from 0% to 35% and reported that the stiffness increases with PEG percentage. These contradicting results warrant further investigation of the effects of PEG concentration on microbubble dynamics to provide a better understanding in designing microbubbles with appropriate qualities for specific imaging and drug delivery applications.

Here, we synthesized perfluorocarbon microbubbles with varying PEG concentrations in their lipid shells. We acoustically characterized them using attenuation to examine the change in their shell properties, specifically interfacial elasticity, relating the changes to the conformation of PEG molecules absorbed at the gas-liquid interface. We also investigated the time evolution of the dissolution of microbubbles dispersed inside the air-saturated water, relating the observed behaviors to the change in shell permeability with increasing PEG concentrations.

METHODS

Preparation and characterization of lipid-coated microbubbles

The synthesis of lipid-shelled microbubbles with perfluorobutane (PFB) gas cores has been described by our group previously (Aliabouzar et al. 2016; Osborn et al. 2019). Briefly, 1,2-dipalmitoyl-*sn*-glycero-3-phosphatidylcholine (DPPC) and 1,2-dipalmitoyl-*sn*-glycero-3-phosphatidylethanolamine-polyethyleneglycol-2000 (DPPE-PEG-2000) (Avanti Polar Lipids, Alabaster, AL, USA) were used to create microbubbles with different shell compositions by varying the ratio of DPPE-PEG-2000 to DPPC (Table 1) along with a PFB (FluoroMed L.P., Round Rock, TX, USA) core. First, the desired amount of lipid powders was dissolved in propylene glycol at 50˚C (above the transition temperature of DPPC) and stirred for 60 min to ensure proper mixing of lipids. Note that different ways of handling lipid were found to affect the microstructure in the lipid shell. First dissolving the lipids in propylene glycol, as adopted here (called an indirect method), in contrast to direct dispersion in the aqueous medium, leads to less structural heterogeneity and a more liquid-condensed (LC) area in the coating (Langeveld et al. 2020). After attainment of a clear solution, a mixture of phosphate-buffered saline (PBS) and glycerol was added. The final mixture containing 10 mg of lipids in 10 mL of an aqueous mixture of PBS, glycerol and propylene glycol in a 80:5:15 volume ratio was stirred for an additional 60 min at 50˚C. The mixture

Table 1. Shell formulations of microbubbles

Name	Shell composition (molar ratio)		Distance between PEG chains (nm)	Configuration
	DPPE-PEG2000 (mol%)	DPPC(mol%)		
0% PEG	0	100	—	—
2% PEG	2	98	5	Mushroom
5% PEG	5	95	3.2	Mushroom-brush border
10% PEG	10	90	2.4	Brush
20% PEG	20	80	1.5	Dense brush

DPPE-PEG2000 = 1,2-dipalmitoyl-*sn*-glycero-3-phosphoethanolamine-polyethylene glycol-2000; DPPC = dipalmitoylphosphatidylcholine; PEG = polyethylene glycol.

was allowed to cool down at room temperature and stored at 4°C for further use.

Microbubbles were made using a mechanical agitation method. First, 1.5-mL aliquots of the lipid solution were placed in 2-mL glass vials (Med Lab Supply, FL, USA). After vial was sealed and clamped with a rubber head and metal cap (Med Lab Supply, FL, USA), the air inside the vial was removed and replaced with PFB. A vial mixer (VIALMIX, Lantheus, Billerica, MA, USA) was used to shake the vial at high frequency for 45 s to produce the microbubble suspensions. The resultant microbubbles were allowed to rest at 4°C for 15 min before experiments.

Inverted optical microscopy (Amscope, Irvine, CA, USA) was used to measure the size distribution and total concentration of the microbubbles following a method described in the literature (Sennoga et al. 2010, 2012, 2015). A 10-μL aliquot of 50× diluted microbubble solution in PBS was inserted in a hemocytometer (VWR, Swedesboro, NJ, USA). A CCD camera (Amscope) connected to an objective lens of 40× magnification with an optical resolution of 580 nm (for the wavelength of 700 nm) was used to capture optical images with a pixel size of 60 nm. ImageJ software (https://imagej.nih.gov/ij/) was used for counting and determining the size distribution of microbubbles. Using the printed grid on the hemocytometer, one can calibrate the pixel-to-distance ratio and calculate the scanned area. Therefore, with knowledge of the depth of the counting chamber (100 μm in this experiment), the volume of the scanned region was obtained. The total concentration is reported as the average number of microbubbles in the respective scanned region volume. For each measurement, at least nine images from different regions of the counting chamber were processed, and more than 1300 microbubbles were counted. This procedure was replicated at least three times, using a new batch of microbubbles each time.

Determination of PEG chain configuration

To determine the configuration of PEG chains, the distance between chains and the Flory radius of the grafted PEG was calculated as (Kenworthy et al. 1995; Abou-Saleh et al. 2014)

$$R_F = aN^{3/5},\ D = \sqrt{A_{lipid}/m} \quad (1)$$

where R_F is the Flory radius, a is the monomer size (0.35 nm for PEG2000) and N is the number of monomer units per chain, which is 45 for PEG2000. D is the distance between chains, A_{lipid} is the area per lipid molecule (0.5 nm^2) (Abou-Saleh et al. 2014) and m is the molar fraction of the PEG in the shell. The Flory radius (R_F) calculated for the DPPC and DPPE-PEG2000 system is roughly 3.4 nm. The distance between chains (D) and corresponding configuration are listed in Table 1. PEG chains form a mushroom-like configuration when the distance between them is greater than the Flory radius ($D > R_F$). As the distance between the chains becomes smaller than the Flory radius ($D < R_F$) the PEG chains are forced to stretch and form a brush configuration. The different concentrations and their configurations are listed in Table 1. We refer to 10% and 20% as in a "brush regime" and the others as in a "mushroom regime." Note that the aforementioned analysis assumes a uniform distribution of PEG chains over the surface of a microbubble, which is only approximately true on average because of phase separations in the lipid shell and the microstructural inhomogeneity, observed in experiments (Langeveld et al. 2020, 2021). Such structural inhomogeneity depends on lipid handling, chemical composition and cooling rate (Borden et al. 2006). However, note that an experimental determination of Langmuir isotherm offered a reasonable match with the theoretical transition threshold using the above analysis in a similar binary (DPPC−DSPE-PEG2000) (and even ternary) system with phase separation (Langeveld et al. 2020). It gives us confidence in the method of determining the phase behaviors of our system. However, we should note that because of phase separation and resulting non-uniform PEG distributions, areas of brush conformation are possible for PEG percentages lower than the nominal brush-mushroom transition value.

Attenuation measurement

Frequency-dependent attenuation of the microbubble solution was measured using the custom setup

illustrated in Figure 1. A desired aliquot of microbubbles was dispersed in de-ionized (DI) water to ensure limited damping and a signal above the noise level. The final numbers of bubbles per milliliter employed in the sample chamber were 74,000 (0% PEG), 58,000 (2% PEG), 64,000 (5% PEG), 142,000 (10% PEG) and 96,000 (20% PEG). To ensure a homogenous distribution of microbubbles, measurements were done 30 s after the injection of microbubbles into the chamber, and a magnetic bar was gently stirring the suspension inside a polycarbonate rectangular chamber throughout the experiments. All experiments were performed at room temperature.

Unfocused single-element transducers (Olympus NDT Corp., Waltham, MA, USA) with central frequencies of 2.25 MHz (−6 dB: 1.6−3.28 MHz) and 5 MHz (−6 dB: 3.2−6.4 MHz) were driven by a pulser-receiver (5800PR, Panametrics-NDT, Waltham, MA, USA) in pulse-echo mode to send and receive pulses with a 100-Hz pulse repetition frequency (PRF). The driving pulse was a negative impulse resulting in a short acoustic pulse of about 1 μs in temporal duration. An external attenuator was used to keep the peak excitation pressure sufficiently small, 17.4 and 18.2 kPa for the 2.25- and 5-MHz transducers, respectively, to guarantee linear dynamics. Previous studies have determined attenuation to be independent of the acoustic pressure and the central frequency of the transducer for this pressure range (Chatterjee et al. 2005b; Raymond et al. 2014; Shekhar et al. 2018). Here also we have studied the effects of different peak acoustic pressures to obtain little variation in the range 9−40 kPa (seen in Fig. 3C, 3D). A bandpass filter was applied from 100 kHz to 35 MHz. An oscilloscope (Tektronix, MDO3024, Beaverton, OR, USA) then gated the received signal with a delay time of 73 μs, which is the time for the acoustic wave to travel the width of the sample chamber forward and back and digitized at a sampling rate of 1.5 GHz. Fifty signals were acquired in averaging mode (64 sequences) and then recorded by an in-house MATLAB (The MathWorks, Natick, MA, USA) code for further processing. Measurement with each formulation was repeated with a fresh sample of suspension at least three times.

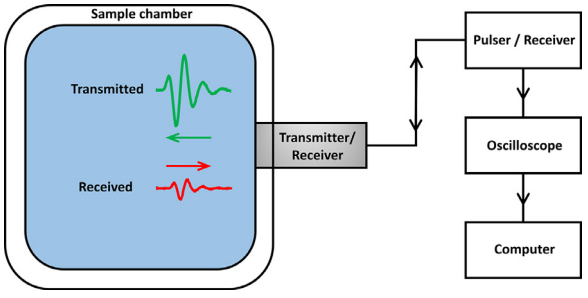

Fig. 1. Experimental setup to measure ultrasound attenuation in a dispersion of microbubbles in de-ionized water.

Attenuation analysis assumes a sufficiently small excitation to ensure a linear propagation of sound with no non-linear transfer across different frequencies. Therefore, each frequency ω component has its independent attenuation $\alpha(\omega)$ (Chatterjee et al. 2005b). To compute it, the signals were taken before and after injection of microbubbles in DI water. The response in the frequency domain was calculated by taking the fast Fourier transform (FFT) of the recorded voltage-time signals. The frequency-dependent attenuation coefficient (dB/cm) was calculated as

$$\alpha(\omega) = 10\log\left(V^2{}_{\text{control}}(\omega)/V^2{}_{\text{bubble}}(\omega)\right)/d \tag{2}$$

where V_{control} and V_{bubble} are the responses without and with microbubbles in the frequency domain, respectively, and d is the propagation length. The amplitudes are squared to account for the relationships between ultrasound intensity, pressure amplitude and voltage amplitude.

Modeling attenuation and interfacial parameter estimation

We use a strain-softening interfacial rheological model, the exponential elasticity model (EEM) developed in our laboratory (Paul et al. 2010) for the encapsulation. We introduce it to the incompressible Rayleigh−Plesset type of equation of bubble dynamics:

$$\rho\left(R\ddot{R}+\frac{3}{2}\dot{R}^2\right) = P_{G0}\left(\frac{R_0}{R}\right)^{3k}\left(1-3k\frac{\dot{R}}{c}\right) - 4\mu\frac{\dot{R}}{R} - \frac{4\kappa^s\dot{R}}{R^2} - \frac{2\gamma(R)}{R} - P_0 + P_A sin\omega t,$$
$$\gamma(R) = \gamma_0 + E^s\beta,\ E^s = E_0^s e^{-\alpha^s\beta},\ \beta = (R/R_E)^2 - 1 \tag{3}$$

Here, ρ is the density, μ the viscosity and c the speed of sound in the liquid. $R(t)$ is the instantaneous radius of the oscillating bubble, R_0 is the initial radius of the bubble and R_E is the radius of the bubble in its unstressed state. P_{G0} is the initial gas pressure of the core of the bubble, k the polytropic constant, P_0 the ambient pressure and P_A the amplitude of the sinusoidal ultrasound excitation with an angular frequency ω. The coating is characterized under the EEM model by the surface tension γ_0, the interfacial viscosity κ^s and the interfacial dilatational elasticity E^s, with the latter defined by the reference elasticity E_0^s and the strain-softening parameter α^s. Under sufficiently low excitation, the oscillation is small enough to warrant a linearization of the Rayleigh−Plesset equation (3) to obtain a simple harmonic oscillator with a resonance frequency ω_0:

$$\omega_0^2 = \frac{1}{\rho R_0^2}\left[3kP_0 + \frac{2E_0^s}{R_0}\left(\frac{\eta}{\alpha^s}\right)(1+2\alpha^s-\eta)\right],\ \eta = \sqrt{1+\frac{4\gamma_0\alpha^s}{E_0^s}} \tag{4}$$

Different models of the coating give rise to different expressions for effective surface tension $\gamma(R)$and the surface dilatational viscosity $\kappa^s(R)$ (Katiyar and Sarkar 2011; Paul et al. 2013). The Marmottant model (MM) (Marmottant et al. 2005) defines the surface tension term in (3) as $\gamma(R) = \gamma(R_0) + \chi[(R/R_0)^2 - 1]$ in a radius range $(R_{\text{buckle}}, R_{\text{rupture}})$. The surface tension becomes zero below $R_{\text{buckle}}$and assumes the value of the pure air-water interface above R_{rupture}. Note that the model is identical in the above range to the constant elasticity model proposed by us (Sarkar et al. 2005), with χ being identical to a constant dilatational elasticity E_0^s. Assuming that the oscillation remains entirely in the linear regime, we obtain a resonance frequency for MM:

$$\omega_0^2 = \frac{1}{\rho R_0^2}\left[3kP_0 + (3k-1)\frac{2\gamma(R_0)}{R_0} + \frac{4\chi}{R_0}\right] \tag{5}$$

For both models the damping term δ is the same:

$$\delta = \frac{1}{\rho\omega_0 R_0^2}\left(4\mu + 4\frac{\kappa^s}{R_0} + \frac{3kP_0\mathrm{R}_0}{c}\right) \tag{6}$$

Accordingly, the attenuation $\alpha(\omega)$ is obtained in terms of the individual extinction cross-section σ_e of a microbubble of initial radius R_0 by integrating over the bubble size distribution:

$$\alpha(\omega) = 10\log e\int_{R_{\min}}^{R_{\max}} \sigma_e(R;\omega)n(R)dR$$
$$\sigma_e = 4\pi R_0^2\frac{c\delta}{\omega_0 R_0}\frac{\Omega^2}{\left[\left(1-\Omega^2\right)^2 + \Omega^2\delta^2\right]}, \Omega = \frac{\omega_0}{\omega} \tag{7}$$

where $n(R)dR$ is the number of the bubbles with a radius between R *and* $R + dR$ in the range $(R_{\min}, R_{\max})$ per unit volume. The experimental attenuation curve obtained from eqn (2) was compared with the theoretical value from eqn (7) to formulate an error function. The error function was minimized using a MATLAB program to obtain the interfacial rheological parameters. The values were changed until the summed squared error between the measured and calculated attenuation curves doubles to obtain the confidence intervals listed in Table 2 and Figure 6 (Hoff et al. 2000).

Microbubble stability

We investigated the stability of microbubbles in suspension by monitoring the change in the attenuation curve over a time interval. The frequency-dependent attenuation was measured every 2 min for 60 min with the acoustic excitation turned on during the time at 100-Hz PRF, and the suspension was stirred continuously. Here, we use a 5-MHz transducer that has a sufficiently broad range to capture the bubble behaviors evolving over the entire time interval. For each sampling time, we compute the total attenuation $A(t)$ summing over all frequencies in eqn (2) as

$$A(t) = 10\log\left(\frac{\sum_\omega V^2_{\text{control}}(\omega)}{\sum_\omega V^2_{\text{bubble}}(\omega)}\right)/d \tag{8}$$

RESULTS AND DISCUSSION

Characterization of microbubbles

Optical microscopy was used to measure the size distribution of the microbubbles. Figure 2A−E illustrate the microbubble size distributions for each shell composition. Because of optical resolution limitations (Sennoga et al. 2010, 2012), only microbubbles larger than 0.6 μm were counted. A bin width of 0.1 μm was used to plot the histograms. There are slight variations in the size distributions from different PEG concentrations. However, the mean diameter of microbubbles for different samples was ~2.2−2.6 μm as can be seen in Figure 2, with about 80%−86% of the total bubbles in any sample having a radius between 1 and 4 μm. The polydispersity of the size distributions was characterized by computing Span = $(D_{90} - D_{10})/D_{50}$ (noted in Fig. 2),

Table 2. Material properties of the shells with different molar ratios of DPPE-PEG2000 mixed with base lipid DPPC

PEG molar ratio (%)	Shell elasticity(N/m)		Shell viscosity($\times 10^{-8}$ N·s/m)		α (EEM)	γ_0 (N/m) (EEM)
	E_0^s (EEM)	χ (MM)	κ^s (EEM)	κ_s (MM)		
0	1.19 [1.14−1.24]	1.21 [1.16−1.27]	1.21 [1.07−1.38]	1.21 [1.07−1.38]	1.7 [0−4.3]	0.011 [0−0.035]
2	1.25 [1.22−1.28]	1.28 [1.25−1.31]	2.88 [2.79−2.96]	2.88 [2.8−2.96]	1.7 [0.5−2.9]	0.012 [0−0.024]
5	1.39 [1.27−1.52]	1.42 [1.3−1.55]	2.34 [2.0−2.7]	2.35 [1.99−2.71]	2.0 [0.6−3.4]	0.013 [0−0.07]
10	0.54 [0.48−0.59]	0.54 [0.49−0.60]	4.01 [3.68−4.37]	4.01 [3.68−4.37]	1.8 [0−7.3]	0.005 [0−0.057]
20	0.67 [0.61−0.73]	0.68 [0.62−0.74]	3.51 [3.09−3.93]	3.51 [3.07−3.94]	1.4 [0−6.1]	0.007 [0−0.052]

DPPE-PEG2000 = 1,2-dipalmitoyl-*sn*-glycero-3-phosphoethanolamine-polyethylene glycol-2000; DPPC = dipalmitoylphosphatidylcholine; EEM = exponential elasticity model; MM = Marmottant model (Marmottant et al. 2005); PEG = polyethylene glycol. Confidence intervals are indicted in [...].

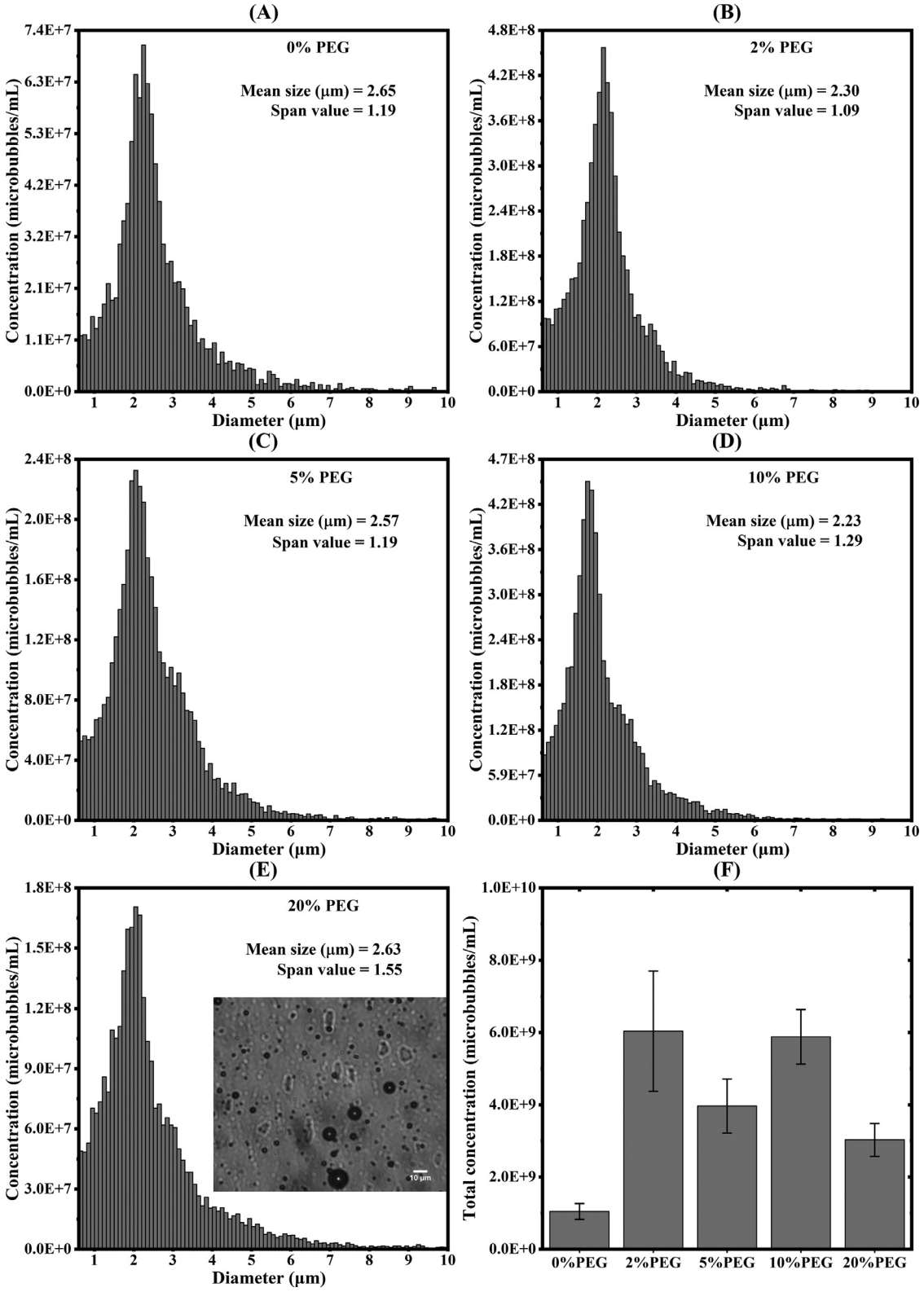

Fig. 2. Size distribution of microbubbles with (A) 0% PEG, (B) 2% PEG, (C) 5% PEG, (D) 10% PEG and (E) 20% PEG. The corresponding number-weighted mean size and span value of the distribution are at the top right corner of each panel. A photograph of 20% microbubbles under a microscope is provided as an example. (F) Total concentration (microbubbles/milliliter) as a function of the PEG percentage in microbubble shell. Concentration reaches a maximum at 2% PEG. Further addition of PEG is accompanied by a decrease in the total microbubble concentration. PEG = polyethylene glycol.

where D_n is the diameter with n% of the total microbubbles below this size, leading to values very similar to those previously obtained in similar preparation methods (Langeveld et al. 2020, 2021). Previously, Dicker et al. (2013a) reported no significant change in the size distribution of DSPC-based microbubbles with varying molar ratios and molecular weights of DSPE-PEG emulsifiers.

Figure 2F illustrates microbubble yield as a function of PEG concentration. The addition of PEG as an emulsifier to the lipid shell resulted in a 10-fold increase in the total concentration in comparison to 0% PEG. Microbubbles with 2% PEG in the shell had the highest number concentration (6.04×10^9 microbubbles /mL). The steric hindrance caused by PEG chains helps to increase the yield in microbubble production by inhibiting the coalescence (Chen and Borden 2010). Further addition of PEG resulted in an approximately 50% reduction in the total concentration, a trend also observed by Abou-Saleh et al. (2014). They found that the microbubble yield reached a maximum at shell compositions of 5% DSPE-PEG2000 and 95% DPPC, and further addition of emulsifiers caused a gradual decrease in the total concentration. The decrease in the concentration was attributed to a disruption in base lipid structure caused by increased repulsive forces between PEG chains.

Attenuation measurements

Figure 3A and 3B illustrate example voltage-time signals and the corresponding power spectra before and after injection of microbubbles (10% PEG for the 2.25-MHz transducer and 2% PEG for the 5-MHz transducer) into the sample chamber. With the microbubble concentrations used, they are typically separated from each other by more than 200 microbubble radii. Figure 3C and 3D plot attenuation for the same cases with varying peak acoustic pressure amplitude. They illustrate that attenuation is insensitive, as it should be, to a slight variation in the peak pressure amplitude range (Chatterjee et al. 2005b; Raymond et al. 2014; Shekhar et al. 2018). As noted, all experiments were performed with 17.4 and 18.2 kPa for the 2.25- and 5-MHz transducers, respectively.

The frequency-dependent attenuation coefficients measured for different PEG concentrations are illustrated in Figure 4A and 4B. Typically the maximum attenuation occurs at an excitation frequency close to the microbubble resonance frequency. Here, a polydisperse

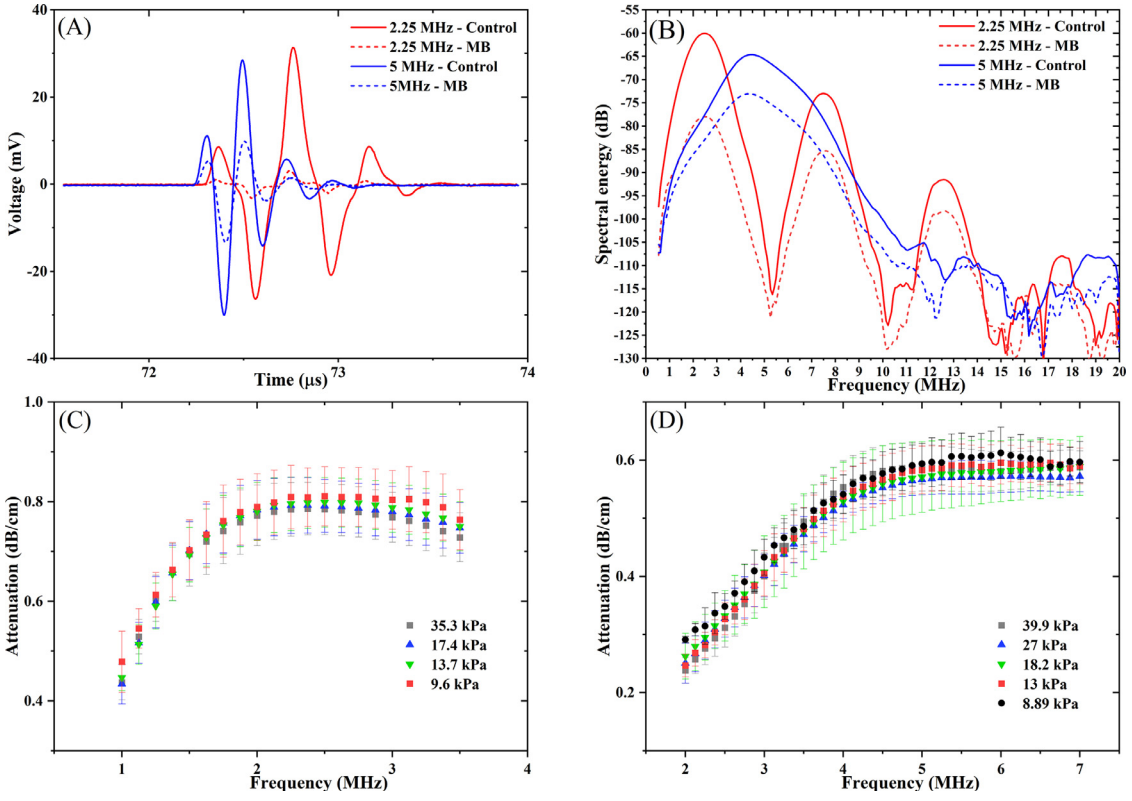

Fig. 3. (A) Example voltage-time signals and (B) power spectrum of received signals before (control) and after injection of microbubbles (MB) into the sample chamber. Attenuation curves were measured using 2.25-MHz (C) and 5-MHz (D) transducers at varying acoustic amplitudes.

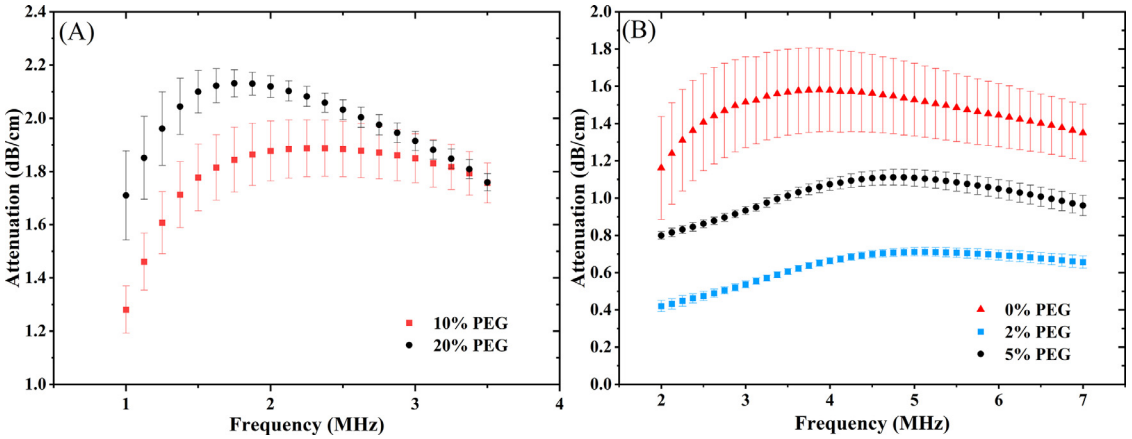

Fig. 4. Frequency-dependent attenuation for (A) 10% and 20% PEG measured at 2.25-MHz center frequency and (B) 0%, 2% and 5% PEG samples measured at 5-MHz center frequency. Although microbubbles in the brush regime resonate at frequencies between 1 and 2 MHz, microbubbles in the mushroom regime resonate at higher frequencies (4−6 MHz). PEG = polyethylene glycol.

bubble population resulted from the mechanical agitation method, and the broad peak represents a weighted average of the resonance frequencies of different-sized bubbles (Kumar and Sarkar 2015) and therefore is representative of the resonance frequency corresponding to that particular microbubble formulation. Microbubbles with higher PEG percentages (Fig. 4A), which fall into the brush regime (Table 1), resonate at lower frequencies—between 1.5 and 2 MHz—while microbubbles with lower PEG percentages (Fig. 4B), corresponding to the mushroom regime, resonate at relatively higher frequencies—between 4 and 6 MHz. Equation (4) indicates that the initial size and surface elasticity play critical roles in determining the resonance frequency. As the size distribution of the microbubbles does not vary significantly for different PEG concentrations (see Characterization of Microbubbles), the difference in resonance frequency for different shell compositions is caused mainly by the difference in shell elasticity.

Material property estimation

Analyzing the measured attenuation using the bubble dynamics model, we estimate the material properties of the shell. Figure 5 illustrates the EEM model fitted to the experimental attenuation data. The estimated values for the material properties of all samples are summarized in Table 2. Previously, the EEM model was used to estimate the material properties of commercial phospholipid-shelled microbubbles such as Definity (Kumar and Sarkar 2015), Sonazoid (Paul et al. 2014) and Targestar P (Kumar and Sarkar 2016) with comparable values for the properties. The interfacial elasticity value changes drastically among microbubbles with different shell materials (Paul et al. 2013). Here, the interfacial elasticity of the shell for 0%, 2% and 5% PEG, all in the

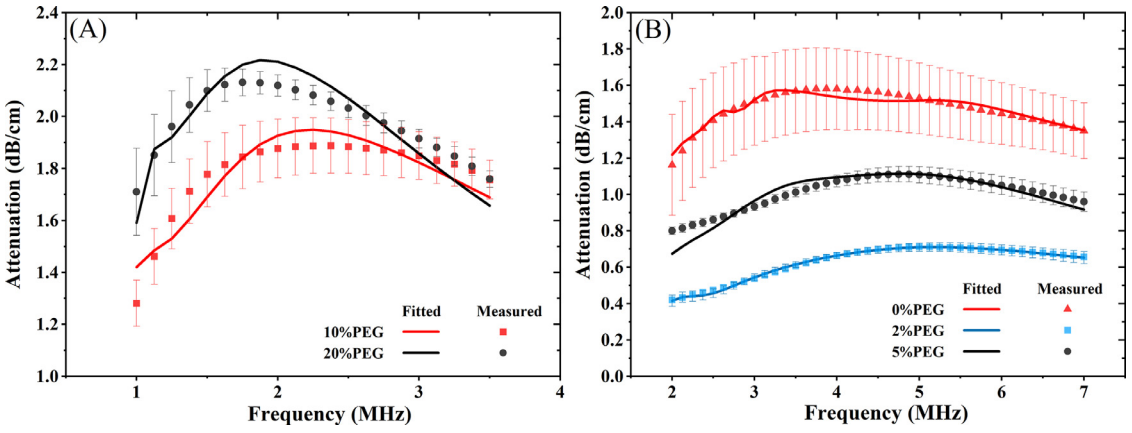

Fig. 5. Exponential elasticity model applied to experimental attenuation data to estimate shell material properties. (A) 10% and 20% PEG. (B) 0%, 2% and 5% PEG. PEG = polyethylene glycol.

mushroom regime, is significantly higher than that for 10% and 20% PEG in the brush regime. However, within each conformational regime, the change in the PEG molar faction does not affect the stiffness of the shell. For comparison, we have also provided the characteristic parameter values according to the MM model in the same Table 2. Following Marmottant et al. (2005), we assumed $\gamma(R_0) = 0$. Note that the similarity of the values between E_0^s and χ, as well as identical values of κ^s between MM and EEM underscore the similarity between the MM and EEM models.

As can be seen from eqn (4), the shell elasticity of coated microbubbles increases the resonance frequency (van der Meer et al. 2007). The estimated values for interfacial elasticity (Table 2 and Fig. 6) correlate well with the peak in the attenuation (Fig. 4A, 4B). Microbubbles with higher PEG concentrations (10% and 20% PEG) in the brush region exhibited resonance peaks at lower frequencies because of the lower estimated shell elasticity. Conversely, the other three (0%, 2% and 5% PEG) in mushroom region with peaks at higher frequencies resulted in higher elasticities.

The observations here are consistent with Dicker et al. (2013b), who found that for DSPC−DSPE-PEG microbubbles, shells with 1% DSPE-PEG-2000 (mushroom regime) had a higher surface dilatational modulus E^s of 2.4 N/m than shells with 7.5% DSPE-PEG-2000 (brush regime, E^s = 1.4 N/m). They also observed the same trend for PEG with higher molecular weights. On the other hand, Segers et al. (2018) reported that the molar ratio of the DPPE-PEG5000 did not affect the stiffness when mixed with DPPC in 5%, 7.5% and 10% molar ratios. However, for DPPE-PEG5000, the number of monomers per chain is 2.5 times higher than that for DPPE-PEG2000, resulting in PEG concentrations greater than ~2% molar ratio forming brush chains (Kenworthy et al. 1995). Therefore, all their configurations were in the brush regime, and the absence of variation in elasticity for them is consistent with our finding. This explanation resolves the apparent difference in trends observed by the two groups for the change in shell elasticity with PEG molar ratio applying an acoustic means of characterization, as is done here. Abou-Saleh et al. (2014) used AFM to mechanically characterize the stiffness of the microbubbles with shells made of DPPC as the base lipid mixed with different percentages of DSPE-B-PEG2000. They observed a slight increase in the effective stiffness with increasing PEG concentrations for molar ratios below 10% and a steep linear increase with higher PEG concentrations. The static compressive stress used in an AFM measurement applied to a single bubble is in sharp contrast to the megahertz frequency acoustic probe and disallows direct comparison.

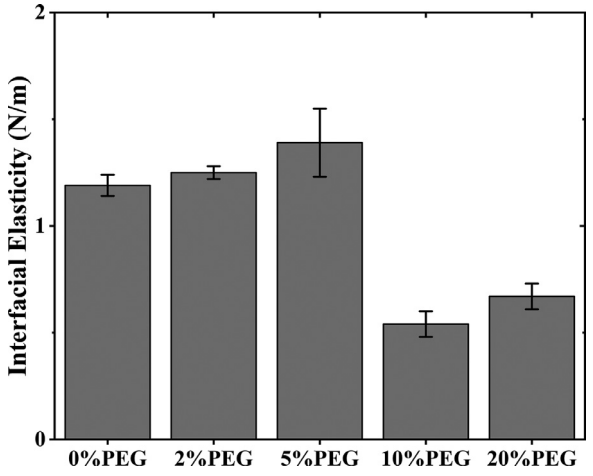

Fig. 6. Interfacial elasticity for microbubbles with different PEG molar fractions in their shells. Limits corresponding to a doubling of the summed error are provided as confidence intervals. PEG = polyethylene glycol.

The decrease in the interfacial dilatational elasticity E^s in the brush region seen here, as well as by (Dicker et al. 2013b), can be explained by the same repulsive force between the PEG chains, which leads to the brush conformation to avoid their mutual overlap. In lipid bilayers with polymer-grafted lipids, Hristova and Needham (1994), using a simplified scaling analysis, determined that such a polymer-polymer repulsive force gives rise to a negative contribution "K_{polymer}" increasing in strength linearly with polymer concentration; that is, it reduces the area expansion elasticity.

The dilatational viscosity κ^s has a higher value in the brush region than in the mushroom region (Table 2). It could be explained by thinking of pegylated lipids as heterogeneity in a 2-D lipid layer continuum. Increasing the concentration of heterogeneities increases the dilatational viscosity, similar to the case of an increase in shear viscosity with particle concentration in bulk suspension rheology (Brady and Bossis 1988), where for a dilute suspension, Einstein's expression of the effective shear viscosity exhibits a linear increase with concentration (Einstein 1906).

Stability of microbubbles

We measured attenuation over a period to investigate the stability of the microbubbles in air-saturated DI water (. In Figure 7A−E, we plot attenuation for each of the compositions, every 6 min over 60 min, illustrating how the frequency-dependent curves evolve. Except for the highest PEG concentration of 20%, all the curves exhibit similar behavior—they are initially broad, over time evolving into ones with a narrow peak, the peak value moving to lower frequencies. Eventually the peak value, as well as the overall attenuation, decreases, but

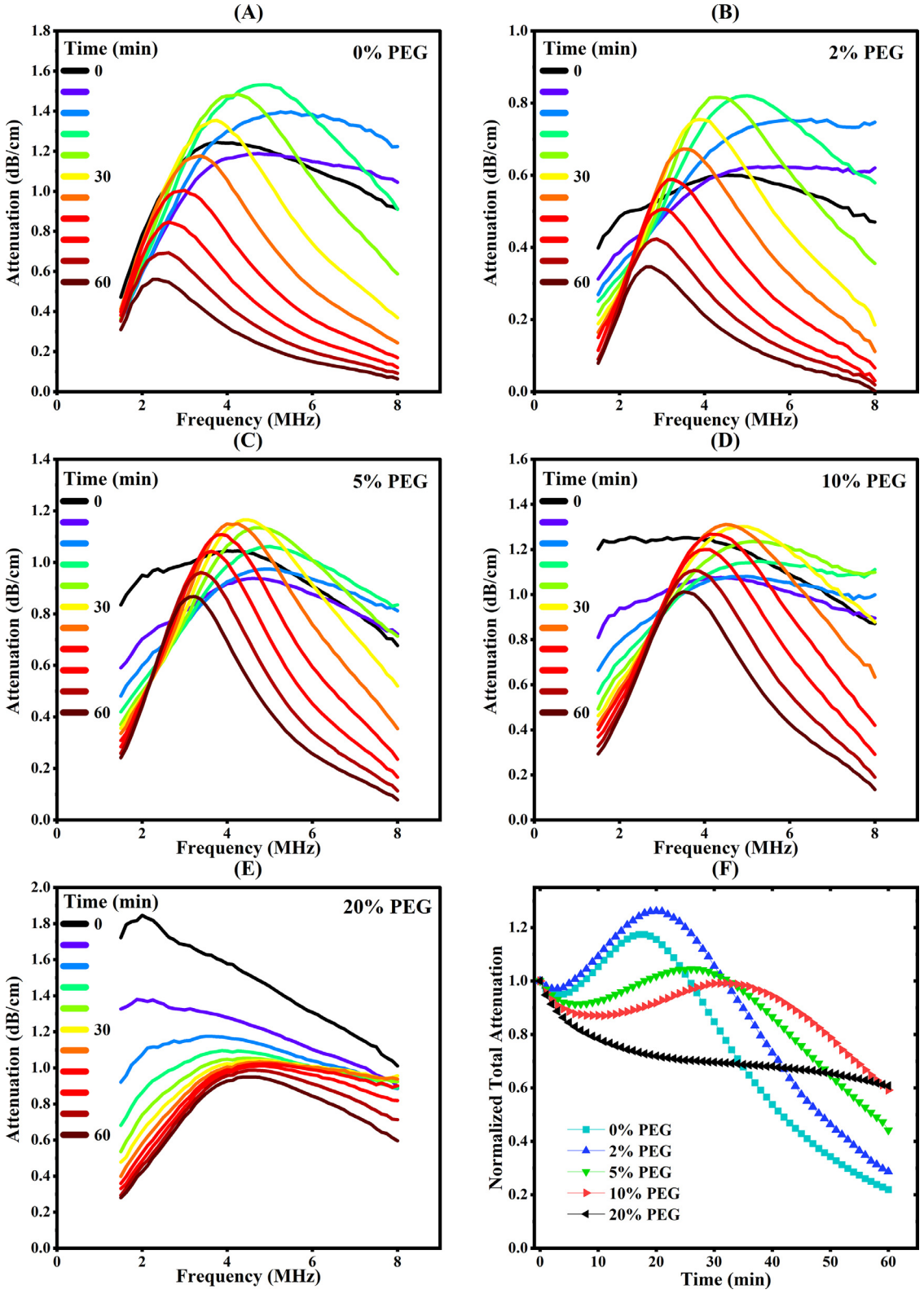

Fig. 7. Frequency-dependent attenuation curves measured at 5 MHz at 6-min intervals for 60 min. (A) 0% PEG. (B) 2% PEG. (C) 5% PEG. (D) 10% PEG. (E) 20% PEG. (F) Normalized total attenuation of microbubble solution as a function of time. PEG = polyethylene glycol.

initially the curves indicate growth, which is clear in the total attenuation (integrated over the frequency domain) plotted in Figure 7F. The total attenuations in that figure have been normalized by their initial values. The figure illustrates that as PEG content increases, the initial increase occurs over longer times, and its magnitude decreases until there is no increase for 20% PEG microbubbles.

The initial growth in the total attenuation and the subsequent reduction seen here are related to the growth of microbubbles resulting from the relatively higher air influx into initially perfluorocarbon-filled microbubbles because of air's higher diffusivity and the lower solubility of perfluorocarbon in water. The decay at later times is due to eventual outward gas diffusion and dissolution. An increase in attenuation initially with time has been noted before by Shi et al. (2000) for Optison and Chatterjee et al. (2005a) for Definity (both perfluorocarbon-based agents), but not for air-filled Albunex agent, which expectedly exhibited only a decay (Hoff 1996; Wu and Tong 1998). In a time-dependent attenuation study over a 10-min (in contrast to the present 60-min) period, Chatterjee et al. (2005a) observed three different amplitude-dependent behaviors: for low amplitudes, total attenuation grew (compare with Fig. 7F); for amplitudes less than 1.2 MPa, total attenuation grew and decayed slowly; but at higher amplitudes, it decayed exponentially, indicating catastrophic shell disruption. A gas diffusion model for this process proposed by our group (Katiyar et al. 2009; Sarkar et al. 2009) exhibited the initial growth caused by the faster influx of air dissolved in the surrounding water with its relatively higher diffusivity compared with the less soluble outflowing perfluorocarbon. Lower gas permeability delays growth and eventual dissolution, the process taking from fractions of a second to hours for different permeabilities (Sarkar et al. 2009). Smaller microbubbles grow and dissolve faster than larger microbubbles, whereas larger ones exhibit bigger initial growth (Katiyar et al. 2009).

Scrutiny of Figure 7A–D reveals that the high-frequency contribution to the attenuation corresponding to smaller bubbles increases very early on (until about 12 min), which also coincides with a slight decrease in total attenuation in Figure 7F. Such an initial shift of the attenuation peak toward high frequency seen also for Sonovue (Li et al. 2018) is due to the larger microbubbles experiencing quick shrinkage at this time and thus increasing the contribution of smaller bubbles. Borden et al. (2005) observed that while larger microbubbles under insonation shrink to a stable size, smaller ones, already at a stable size, do not change much. Also, shrinking of microbubbles compresses the lipid shell, increasing its elasticity and resulting in resonance moving to a higher frequency. Segers et al. (2016) observed a similar shift in attenuation peak to the higher frequency, that is, an increase in the resonance frequency, with time under repeated low-amplitude insonations on monodisperse microbubbles with Definity-like lipid composition (DPPC:DPPA:DPPE-PEG5000 in 80:10:10 molar ratio). They related it to an increase in shell elasticity and discussed lipid shedding as a possible mechanism. Lipid shedding was also implicated in reducing the size of a Definity microbubbles oscillating near resonance under repeated insonations of 100 kPa and 1.6 MHz (Thomas et al. 2012). However, note that the acoustic excitation (~18 kPa) employed here is below the trigger pressure for lipid shedding (85 kPa as reported in the literature [Luan et al. 2014]).

After 12 min, all curves in Figure 7A–D exhibit a shift of peak toward lower frequency and an overall self-similar reduction. This shift to a lower frequency, that is, larger microbubbles, stems from the initial growth of microbubbles caused by enhanced air influx noted above, as well as the slower dissolution of bigger microbubbles. Such a shift in the resonance peak toward lower frequency was observed by Shi and Forsberg (2000) in the first 10 min after injection and then a reversal to the original frequency and a reduction in attenuation. Growth of microbubbles followed by contraction to a single size was also seen in monodisperse microbubbles synthesized in a microfluidic setup (Segers et al. 2016), where the growth was thought to be caused by Ostwald ripening of larger microbubbles at the expense of smaller microbubbles and the eventual shrinkage caused by outward diffusion reaching a stable shape accompanied by a lowering of surface tension in the contracting lipid shell. However, system confinement and therefore the proximity of bubbles facilitated inter-bubble gas transport in that system, which is not the case here with bubbles separated by more than 200 radii.

All the curves exhibited an eventual overall decrease in attenuation with time because of dissolution, the rate of reduction decreasing with increasing PEG percentage (Fig. 7A–F), indicating decreased permeability with increasing PEG. The decreased permeability also contributes to the longer transient growth period for higher PEG microbubbles (Fig. 7F). The highest concentration with 20% PEG in Figure 7E exhibits a steady decrease without growth.

Coalescence can give rise to higher volumes, stronger attenuation, larger bubbles with lower resonance frequencies and, therefore, larger contributions at the low frequencies, which seems to appear in all curves eventually except for the 20% PEG case. Microbubbles in the mushroom regime, with lower PEG concentrations and shorter chains, might be more vulnerable to coalescence because of the lower steric hindrance compared with that

of microbubbles in the brush region. However, because of the large inter-bubble separation for the concentrations considered, coalescence may be rare.

CONCLUSIONS

In this study, lipid-shelled microbubbles synthesized with DPPC and with a varying DPPE-PEG2000 molar fraction as an emulsifier were studied. It is well known that increasing the PEG concentration leads to a transition from their mushroom configuration at the absorbed interface to a brush configuration. Five different shell concentrations with roughly three in mushroom and two in brush configurations have been investigated using acoustic attenuation experiments. We observed that microbubbles with their shells in brush and mushroom regimes exhibit distinct behaviors. A non-linear strain-softening interfacial rheological model (EEM) was used to characterize the five different microbubble formulations determining the rheological properties of the shell monolayer. The interfacial elasticity of microbubbles with their shells in the mushroom regime is significantly higher than that of microbubbles with their shells in the brush regime. Microbubbles with varying concentrations but in the same configuration regime did not exhibit significant variations in their shell properties. We also studied time-dependent attenuation to investigate the stability and evolution of microbubbles in air-saturated water under acoustic excitation. Our results indicated that the microbubbles with the highest PEG concentration of 20%, and thereby in a dense brush conformation, behave differently from the other microbubbles. The lower PEG microbubbles exhibited non-monotonic behavior in total attenuation: first a very small decrease accompanying a shift in the attenuation peak toward higher frequency, then a transient increase in total attenuation and shift of the peak to lower frequency because of higher air influx into perfluorocarbon microbubbles and an eventual overall decrease. The 20% PEG microbubbles exhibited a steady decrease in total attenuation. With increasing PEG content, the dynamics is slowed with longer transient growth and slower decay. The evolution is seen to be a result of different permeability critically affected by the PEG conformation, which in turn changes the dynamics of the size change. Overall, the shell composition, specifically the PEG concentration and the resulting conformations, play a significant role in the acoustic behavior of microbubbles.

Acknowledgments—K.S. and S.M. acknowledge partial support from National Institutes of Health Award R01 GM114080. K.S. acknowledges partial support from National Science Foundation Award 2037849.

Conflict of interest disclosure—The authors declare they have no conflicts of interest.

REFERENCES

Abou-Saleh RH, Swain M, Evans SD, Thomson NH. Poly(ethylene glycol) lipid-shelled microbubbles: abundance, stability, and mechanical properties. Langmuir 2014;30:5557–5563.

Aliabouzar M, Zhang LG, Sarkar K. Lipid coated microbubbles and low intensity pulsed ultrasound enhance chondrogenesis of human mesenchymal stem cells in 3D printed scaffolds. Sci Rep 2016;6:37728.

Azmin M, Harfield C, Ahmad Z, Edirisinghe M, Stride E. How do microbubbles and ultrasound interact? Basic physical, dynamic and engineering principles. Curr Pharm Des 2012;18:2118–2134.

Borden MA, Kruse DE, Caskey CF, Zhao S, Dayton PA, Ferrara KW. Influence of lipid shell physicochemical properties on ultrasound-induced microbubble destruction. IEEE Trans Ultrason Ferroelectr Freq Control 2005;52:1992–2002.

Borden MA, Martinez GV, Ricker J, Tsvetkova N, Longo M, Gillies RJ, Dayton PA, Ferrara KW. Lateral phase separation in lipid-coated microbubbles. Langmuir 2006;22:4291–4297.

Brady JF, Bossis G. Stokesian dynamics. Annu Rev Fluid Mech 1988;20:111–157.

Chatterjee D, Sarkar K. A Newtonian rheological model for the interface of microbubble contrast agents. Ultrasound Med Biol 2003;29:1749–1757.

Chatterjee D, Jain P, Sarkar K. Ultrasound-mediated destruction of contrast microbubbles used for medical imaging and drug delivery. Phys Fluids 2005a;17 100603.

Chatterjee D, Sarkar K, Jain P, Schreppler NE. On the suitability of broadband attenuation measurement for characterizing contrast microbubbles. Ultrasound Med Biol 2005b;31:781–786.

Chen CC, Borden MA. Ligand conjugation to bimodal poly(ethylene glycol) brush layers on microbubbles. Langmuir 2010;26:13183–13194.

de Gennes PG. Polymers at an interface: A simplified view. Adv Colloid Interface Sci 1987;27:189–209.

de Jong N, Bouakaz A, Frinking P. Basic acoustic properties of microbubbles. Echocardiography 2002;19:229–240.

Dicker S, Mleczko M, Schmitz G, Wrenn SP. Size distribution of microbubbles as a function of shell composition. Ultrasonics 2013a;53:1363–1367.

Dicker S, Mleczko M, Siepmann M, Wallace N, Sunny Y, Bawiec CR, Schmitz G, Lewin P, Wrenn SP. Influence of shell composition on the resonance frequency of microbubble contrast agents. Ultrasound Med Biol 2013b;39:1292–1302.

Doinikov AA, Bouakaz A. Review of shell models for contrast agent microbubbles. IEEE Trans Ultrason Ferroelectr Freq Control 2011;58:981–993.

Einstein A. Eine neue bestimmung der Molekul-dimension. Ann Phys 1906;19:289–306.

Helfield B. A review of phospholipid encapsulated ultrasound contrast agent microbubble physics. Ultrasound Med Biol 2019;45:282–300.

Hoff L. Acoustic properties of ultrasonic contrast agents. Ultrasonics 1996;34:591–593.

Hoff L, Sontum PC, Hovem JM. Oscillations of polymeric microbubbles: Effect of the encapsulating shell. J Acoust Soc Am 2000;107:2272–2280.

Hristova K, Needham D. The influence of polymer-grafted lipids on the physical properties of lipid bilayers: A theoretical study. J Colloid Interface Sci 1994;168:302–314.

Katiyar A, Sarkar K. Excitation threshold for subharmonic generation from contrast microbubbles. J Acoust Soc Am 2011;130:3137–3147.

Katiyar A, Sarkar K, Jain P. Effects of encapsulation elasticity on the stability of an encapsulated microbubble. J Colloid Interface Sci 2009;336:519–525.

Kenworthy AK, Hristova K, Needham D, McIntosh TJ. Range and magnitude of the steric pressure between bilayers containing phospholipids with covalently attached poly(ethylene glycol). Biophys J 1995;68:1921–1936.

Kooiman K, Vos HJ, Versluis M, de Jong N. Acoustic behavior of microbubbles and implications for drug delivery. Adv Drug Deliv Rev 2014;72:28–48.

Kumar KN, Sarkar K. Effects of ambient hydrostatic pressure on the material properties of the encapsulation of an ultrasound contrast microbubble. J Acoust Soc Am 2015;138:624–634.
Kumar KN, Sarkar K. Interfacial rheological properties of contrast microbubble Targesar P as a function of ambient pressure. Ultrasound Med Biol 2016;42:1010–1017.
Kwan JJ, Borden MA. Microbubble dissolution in a multigas environment. Langmuir 2010;26:6542–6548.
Langeveld SAG, Schwieger C, Beekers I, Blaffert J, van Rooij T, Blume A, Kooiman K. Ligand distribution and lipid phase behavior in phospholipid-coated microbubbles and monolayers. Langmuir 2020;36:3221–3233.
Langeveld SAG, Beekers I, Collado-Lara G, van der Steen AFW, de Jong N, Kooiman K. The impact of lipid handling and phase distribution on the acoustic behavior of microbubbles. Pharmaceutics 2021;13:119.
Li F, Li D, Yan F. Improvement of detection sensitivity of microbubbles as sensors to detect ambient pressure. Sensors (Basel) 2018;18:4083.
Lozano MM, Longo ML. Complex formation and other phase transformations mapped in saturated phosphatidylcholine/DSPE-PEG2000 monolayers. Soft Matter 2009;5:1822–1834.
Luan Y, Lajoinie G, Gelderblom E, Skachkov I, van der Steen AF, Vos HJ, Versluis M, De Jong N. Lipid shedding from single oscillating microbubbles. Ultrasound Med Biol 2014;40:1834–1846.
Lum JS, Dove JD, Murray TW, Borden MA. Single microbubble measurements of lipid monolayer viscoelastic properties for small-amplitude oscillations. Langmuir 2016;32:9410–9417.
Marik J, Tartis MS, Zhang H, Fung JY, Kheirolomoom A, Sutcliffe JL, Ferrara KW. Long-circulating liposomes radiolabeled with [^{18}F] fluorodipalmitin ([^{18}F]FDP). Nuclear Med Biol 2007;34:165–171.
Marmottant P, van der Meer S, Emmer M, Versluis M, de Jong N, Hilgenfeldt S, Lohse D. A model for large amplitude oscillations of coated bubbles accounting for buckling and rupture. J Acoust Soc Am 2005;118:3499–3505.
Mulvana H, Browning RJ, Luan Y, de Jong N, Tang MX, Eckersley RJ, Stride E. Characterization of contrast agent microbubbles for ultrasound imaging and therapy research. IEEE Trans Ultrason Ferroelectr Freq Control 2017;64:232–251.
Osborn J, Aliabouzar M, Zhou X, Rao R, Zhang LG, Sarkar K. Lipid-coated microbubbles: Enhanced osteogenic differentiation of human mesenchymal stem cells using microbubbles and low intensity pulsed ultrasound on 3D printed scaffolds. Adv Biosyst 2019;3 e1800257.
Paul S, Katiyar A, Sarkar K, Chatterjee D, Shi WT, Forsberg F. Material characterization of the encapsulation of an ultrasound contrast microbubble and its subharmonic response: Strain-softening interfacial elasticity model. J Acoust Soc Am 2010;127:3846–3857.
Paul S, Russakow D, Rodgers T, Sarkar K, Cochran M, Wheatley MA. Determination of the interfacial rheological properties of a Poly (DL-lactic acid)-encapsulated contrast agent uning in vitro attenuation and scattering. Ultrasound Med Biol 2013;39:1277–1291.
Paul S, Nahire R, Mallik S, Sarkar K. Encapsulated microbubbles and echogenic liposomes for contrast ultrasound imaging and targeted drug delivery. Comput Mech 2014;53:413–435.
Raymond JL, Haworth KJ, Bader KB, Radhakrishnan K, Griffin JK, Huang SL, McPherson DD, Holland CK. Broadband attenuation measurements of phospholipid-shelled ultrasound contrast agents. Ultrasound Med Biol 2014;40:410–421.
Sarkar K, Shi WT, Chatterjee D, Forsberg F. Characterization of ultrasound contrast microbubbles using in vitro experiments and viscous and viscoelastic interface models for encapsulation. J Acoust Soc Am 2005;118:539–550.
Sarkar K, Katiyar A, Jain P. Growth and dissolution of an encapsulated contrast microbubble: Effects of encapsulation permeability. Ultrasound Med Biol 2009;35:1385–1396.
Sboros V. Response of contrast agents to ultrasound. Adv Drug Deliv Rev 2008;60:1117–1136.
Sboros V, Glynos E, Pye SD, Moran CM, Butler M, Ross J, Short R, McDicken WN, Koutsos V. Nanointerrogation of ultrasonic contrast agent microbubbles using atomic force microscopy. Ultrasound Med Biol 2006;32:579–585.
Segers T, de Rond L, de Jong N, Borden M, Versluis M. Stability of monodisperse phospholipid-coated microbubbles formed by flow-focusing at high production rates. Langmuir 2016;32: 3937–3944.
Segers T, Gaud E, Versluis M, Frinking P. High-precision acoustic measurements of the nonlinear dilatational elasticity of phospholipid coated monodisperse microbubbles. Soft Matter 2018;14:9550–9561.
Sennoga CA, Mahue V, Loughran J, Casey J, Seddon JM, Tang M, Eckersley RJ. On sizing and counting of microbubbles using optical microscopy. Ultrasound Med Biol 2010;36:2093–2096.
Sennoga CA, Yeh JS, Alter J, Stride E, Nihoyannopoulos P, Seddon JM, Haskard DO, Hajnal JV, Tang MX, Eckersley RJ. Evaluation of methods for sizing and counting of ultrasound contrast agents. Ultrasound Med Biol 2012;38:834–845.
Sennoga CA, Kanbar E, Bouakaz A. An ImageJ plugin for the sizing and counting of microbubbles. Proc IEEE Int Ultrason Symp 2015;1–4.
Shekhar H, Smith NJ, Raymond JL, Holland CK. Effect of Temperature on the Size Distribution, Shell Properties, and Stability of Definity®. Ultrasound Med Biol 2018;44:434–446.
Shi WT, Forsberg F. Ultrasonic characterization of the nonlinear properties of contrast microbubbles. Ultrasound Med Biol 2000;26:93–104.
Thomas DH, Butler M, Anderson T, Emmer M, Vos H, Borden M, Stride E, Nd Jong. Sboros V. The “quasi-stable” lipid shelled microbubble in response to consecutive ultrasound pulses. Appl Phys Lett 2012;101 071601.
van der Meer SM, Dollet B, Voormolen MM, Chin CT, Bouakaz A, de Jong N, Versluis M, Lohse D. Microbubble spectroscopy of ultrasound contrast agents. J Acoust Soc Am 2007;121:648–656.
Wu J, Tong J. Experimental study of stability of a contrast agent in an ultrasound field. Ultrasound Med Biol 1998;24:257–265.